Journal of Power Sources 364 (2017) 328–340

Contents lists available at ScienceDirect

Journal of Power Sources

journal homepage: www.elsevier.com/locate/jpowsour

An electrochemical-thermal coupled overcharge-to-thermal-runaway model for lithium ion battery

Dongsheng Ren [a], Xuning Feng [a, b], Languang Lu [a], Minggao Ouyang [a, *], Siqi Zheng [b], Jianqiu Li [a], Xiangming He [a, b]

[a] State Key Laboratory of Automotive Safety and Energy, Tsinghua University, Beijing 100084, China
[b] Institute of Nuclear and New Energy Technology, Tsinghua University, Beijing 100084, China

HIGHLIGHTS

- An electrochemical-thermal coupled overcharge-to-thermal-runaway model is built.
- Adiabatic overcharge tests were conducted using EV-ARC to validate the model.
- The overcharge-to-thermal-runaway model can fit well with the experiment.
- The model help to quantify the heat generation rates of each heat sources.
- Modeling analysis of the parameters helps find solutions for overcharge problem.

GRAPHICAL ABSTRACT

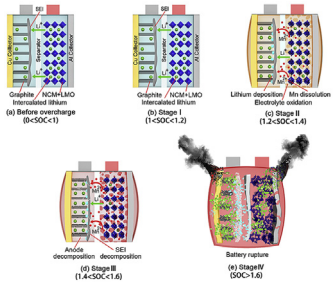

ARTICLE INFO

Article history:
Received 13 June 2017
Received in revised form
8 August 2017
Accepted 11 August 2017
Available online 18 August 2017

Keywords:
Lithium ion battery
Battery safety
Overcharge
Thermal runaway
Electrochemical-thermal coupled model

ABSTRACT

This paper presents an electrochemical-thermal coupled overcharge-to-thermal-runaway (TR) model to predict the highly interactive electrochemical and thermal behaviors of lithium ion battery under the overcharge conditions. In this model, the battery voltage equals the difference between the cathode potential and the anode potential, whereas the temperature is predicted by modeling the combined heat generations, including joule heat, thermal runaway reactions and internal short circuit. The model can fit well with the adiabatic overcharge tests results at 0.33C, 0.5C and 1C, indicating a good capture of the overcharge-to-TR mechanism. The modeling analysis based on the validated model helps to quantify the heat generation rates of each heat sources during the overcharge-to-TR process. And the two thermal runaway reactions including the electrolyte oxidation reaction and the reaction between deposited lithium and electrolyte are found to contribute most to the heat generations during the overcharge process. Further modeling analysis on the critical parameters is performed to find possible solutions for the overcharge problem of lithium ion battery. The result shows that increasing the oxidation potential of the electrolyte, and increasing the onset temperature of thermal runaway are the two effective ways to improve the overcharge performance of lithium ion battery.

1. Introduction

Under the pressure of energy crisis and environmental pollution, new energy vehicles, especially the electric vehicles (EVs)

* Corresponding author.
E-mail addresses: rds14@mails.tsinghua.edu.cn (D. Ren), ouymg@tsinghua.edu.cn (M. Ouyang).

http://dx.doi.org/10.1016/j.jpowsour.2017.08.035
0378-7753/

Nomenclature

Variables

A_x	the frequency factor for the reaction with reactant x (s^{-1})
C_{anode}	the capacity of anode (Ah)
$C_{cathode}$	the capacity of cathode (Ah)
$C_{cathode,0}$	the initial value of $C_{cathode}$ (Ah)
C_p	the specific heat capacity ($J \cdot kg^{-1} \cdot K^{-1}$)
c_x	the normalized concentration of reactant x (1)
$c_{x,0}$	The initial value of c_x (1)
$E_{a,x}$	the activation energy for the reaction with reactant x ($J \cdot mol^{-1}$)
F	the Faraday constant ($C \cdot mol^{-1}$)
I	the overcharge current (A)
i_0	the exchange-current for lithium deposition reaction (A)
i_{Li}	the rate of lithium deposition reaction (A)
$k_{cathode}$	the proportion factor for the cathode decomposition reaction (1)
k_{Mn}	the proportion factor for the Mn dissolution reaction (1)
$k_{electrolyte}$	the proportion factor for the electrolyte oxidation reaction (1)
k_{Li}	the proportion factor for the reaction between deposited lithium and electrolyte (1)
k_Q	the proportion factor for the cathode capacity (1)
M	the mass of the battery (kg)
m_x	the mass of reactant x (g)
n_{Li}	the amount of deposited lithium (mol)
Q	the heat generation rate (W)
Q_e	the heat generation rate originated from massive internal short circuit (W)
Q_{ohm}	the joule heat generation rate (W)
Q_p	the heat dissipation rate (W)
Q_r	the heat generation rate by chemical reaction (W)
Q_{rev}	the reversible entropic heat generation rate (W)
Q_x	the heat generation rate of the reaction with reactant x (W)
R	the ideal gas constant ($J \cdot mol^{-1} \cdot K^{-1}$)
r_{bat}	the internal resistance of the battery (Ω)
r_{SEI}	the resistance caused by the SEI (Solid Electrolyte Interface) film (Ω)
$r_{cathode}$	the resistance caused by the film formed on the cathode surface (Ω)
SOC	the battery state of charge (1)
SOC_{TR}	the battery SOC when thermal runaway happens (1)
T	the battery temperature (°C)
T_0	the initial value of battery temperature (°C)
$T_{onset,TR}$	the onset temperature of thermal runaway (°C)
$T_{onset,x}$	the onset temperature of the reaction with reactant x (°C)
V_{anode}	the anode potential (V)
$V_{cathode}$	the cathode potential (V)
$V_{electrolyte,ref}$	the oxidation potential of the electrolyte (V)
$V_{Mn,ref}$	the dissolution potential of Mn^{3+} (V)
V_{sim}	the simulated battery voltage (V)
x	the lithium content in Li_xC_6 (1)
x_0	the initial value of x (1)
y	the lithium content in the cathode (1)
y_0	the initial value of y (1)
ΔH_e	the total electrical energy released during massive internal short circuit (J)
ΔH_x	the enthalpy for the reaction with reactant x ($J \cdot g^{-1}$)
Δt	the average short circuit time (s)
ΔV	the battery voltage change during the interruption of the charging current (V)

Greek letters

K_x	the rate of the reaction with reactant x (s^{-1})
α_a	the transfer coefficient for the lithium deposition reaction (1)
α_c	the transfer coefficient for the lithium deposition reaction (1)
$\alpha_{electrolyte}$	the transfer coefficient for the electrolyte oxidation reaction (1)
α_{Mn}	the transfer coefficient for the Mn dissolution reaction (1)
v_{Li}	the proportion factor for the calculation of the amount of deposited lithium (mol)

Subscripts

x	denotes that the variable is for reactant x, as listed in Table 2

become increasingly popular throughout the whole world. Lithium ion batteries are the most widely used power sources for electric vehicles, given their high energy, power density and extended cycle life. However, potential safety problems of lithium ion batteries, especially those associated with thermal runaway, have aroused much attention [1–6].

The thermal runaway of lithium ion batteries can be induced by unexpected abuse conditions, such as crush [7], short circuit [8], overheat [9,10] or overcharge [11,12]. Overcharge, as one of the most common field failure, usually occurs when the charge current is forced through after the battery reaches its nominal cut-off voltage [4,13]. The overcharge can be caused by the malfunction of the charger or the inappropriate design of battery management system [14].

The overcharge failure mechanism for lithium ion batteries has been investigated by some researchers [4,11,12,15–22]. Generally, when a battery is overcharged, its temperature quickly rises up due to a large amount of heat generation, including joule heat and the heat generated by a series of side reactions at both cathode and anode [11,22]. The cathode active material suffers from irreversible structural change when over-delithiated [23–25], followed by transitional metal ion (Mn^{2+} etc.) dissolution and active material decomposition [26–29]. The electrolyte will also be oxidized when the cathode potential surpasses the electrolyte oxidation potential [27,30]. The anode potential drops down to below 0 V with full intercalation of lithium, resulting in metallic lithium deposition [27,31–33]. The deposited lithium will react with the electrolyte and thicken the SEI (Solid Electrolyte Interface) film [27,34]. Moreover, those side reactions will also release a large amount of gas, such as CO_2 and H_2O, leading to severe swelling of the battery [15,35,36].

Thermal runaway models were built based on the experimental works to simulate the thermal and electrochemical responses and explore the failure mechanisms of lithium ion batteries under

variant abuse conditions [4,5,7,37–46]. Lumped model and three-dimension model were developed by Hatchard et al. [39] and Kim et al. [42], respectively, to predict the thermal abuse behaviors of the lithium ion batteries under oven tests. In their models, the heat generations from various exothermic reactions were modeled using kinetic equations, i.e. Arrhenius equations [39,42], with the kinetic parameters obtained using accelerating rate calorimetry (ARC) and differential scanning calorimetry (DSC) tests [47–50]. Spotnitz et al. [4] summarized the various kinds of exothermic reaction kinetics for different anode and cathode active materials. Wang et al. [45,46] has analyzed the battery thermal runaway behaviors using Semenov and Frank-Kamenetskii models. Various models have also been developed to investigate the safety behaviors of lithium ion batteries under mechanical and electrical abuse, such as nail penetration [41,51], crush [52–55] and internal short circuit (ISC) [42,56,57] etc. These model-based investigations have promoted theoretical understanding of battery thermal runaway mechanisms beyond what is possible from experiments only and helped to find possible solutions for the safety problems of lithium ion batteries.

For lithium ion batteries under overcharge abuse condition, few researchers have presented models to predict the full overcharge process of lithium ion batteries, but some available researches were conducted on separate reaction kinetics during overcharge. Zeng et al. [11] have established a simple model to analyze the heat generation during the overcharge process. Newman et al. [30] has developed a model to simulate the electrolyte oxidation reaction using Tafel kinetics equation. Arora et al. [34] has built up an electrochemical model to predict the lithium deposition on the graphite anode during overcharge process. Spotnitz et al. [4] has developed a thermal model to investigate the root cause of the overcharge-to-thermal-runaway of lithium ion batteries. However, the electrochemical and thermal behaviors are highly interactive during the overcharge process, accompanied with significant temperature and voltage changes, and these models focused on the separate electrochemical or thermal behaviors can not fully reveal the overcharge failure mechanism of lithium ion batteries. To the best knowledge of the authors, no computational model is available to predict the electrochemical-thermal coupled behaviors of lithium ion batteries under overcharge abuse conditions.

Therefore, in this paper, we firstly establish an electrochemical-thermal coupled overcharge-to-thermal-runaway (TR) model, which not only predicts both of the voltage and temperature responses but also reveals the electrochemical-thermal coupled failure mechanism during overcharge process. In this model, the battery voltage is considered as the difference of the cathode potential and the anode potential, whereas the temperature response is predicted by modeling the combined heat generations, including joule heat, thermal runaway reactions and internal short circuit. Series of overcharge tests were conducted at different overcharge currents under adiabatic conditions using extended volume accelerating rating calorimetry (EV-ARC) to verify the overcharge-to-thermal-runaway model. The heat generation rates of each heat sources during the overcharge-to-TR process are compared quantitatively using the validated model. Moreover, modeling analysis is carried out to discuss possible solutions to improve the overcharge performance of lithium ion battery.

2. Experiment

2.1. Overcharge tests under adiabatic conditions using EV-ARC

Overcharge tests at variant overcharge currents were conducted under adiabatic conditions using the EV-ARC to verify the overcharge-to-thermal-runaway model, as summarized in Table 1. As shown in Fig. 1 (a), EV-ARC manufactured by Thermal Hazard Technology (THT) was used to provide the adiabatic conditions during the overcharge tests. The battery was placed inside the chamber of the EV-ARC, and was connected with a battery cycler (Neware BTS 20V100A), as illustrated in Fig. 1(b). During the overcharge tests, the battery was charged by the battery cycler from SOC(state of charge) = 0. The K-type thermocouples were attached on the battery and connected to a data logger made by Pico Technology. The sampling time intervals of the battery cycler and the data logger were set as 1 s.

A 40 Ah lithium ion battery (240 mm × 150 mm × 14 mm) composed of two pouch cells connected in parallel was utilized in this study, denoted as Cell 1 and Cell 2, as shown in Fig. 1(c) and (d). The battery has $Li_yNi_{1/3}Co_{1/3}Mn_{1/3}O_2$ (NCM) + $Li_yMn_2O_4$ (LMO) composite cathode and graphite anode. The battery configuration of overcharge tests is illustrated in Fig. 1(c) and (d). K type thermocouple No.1 was inserted between Cell 1 and Cell 2 to monitor the internal temperature of the battery during the overcharge process, while thermocouple No.2 was attached on the surface of Cell 1 to record the surface temperature. The internal temperature of the battery recorded by thermocouple No.1 was used for model validation in the following sections. High temperature insulation Kapton tape wrapped around the battery to keep compact contact of the two pouch cells during the overcharge tests.

The internal resistance of the battery was also measured by interrupting the charging current, with 10 s pulse in every 12 min, as shown in Fig. 2. The internal resistance of the battery can be calculated by Eqn. (1), where ΔV is the change of the battery voltage during the interruption of the overcharge current, and I is the overcharge current.

$$r_{bat} = \Delta V/I \tag{1}$$

2.2. Coin cell tests

Overcharge (over-discharge) tests for the cathode (anode) of the battery were conducted to investigate the electrochemical properties of the electrodes under overcharge condition. Coin cells with NCM + LMO/Li and graphite/Li electrodes were assembled using pieces cut from the electrodes of one large format cell. The coin cells with NCM + LMO/Li electrodes were overcharged with a current of 0.5 mA (less than 1/25C), while those with graphite/Li were over-discharged with the same current.

3. Model development

3.1. Overview of the overcharge mechanism

Fig. 3 illustrates the battery voltage, temperature and resistance during the overcharge process. According to the literature, the whole overcharge process for lithium ion batteries with NCM + LMO cathodes can be divided into four stages, as illustrated in Fig. 4, and side reactions happen at each stages can be summarized as follows:

Table 1
The overcharge tests conducted using the EV-ARC.

No.	Overcharge current (C)
1	0.5
2	0.33
3	1

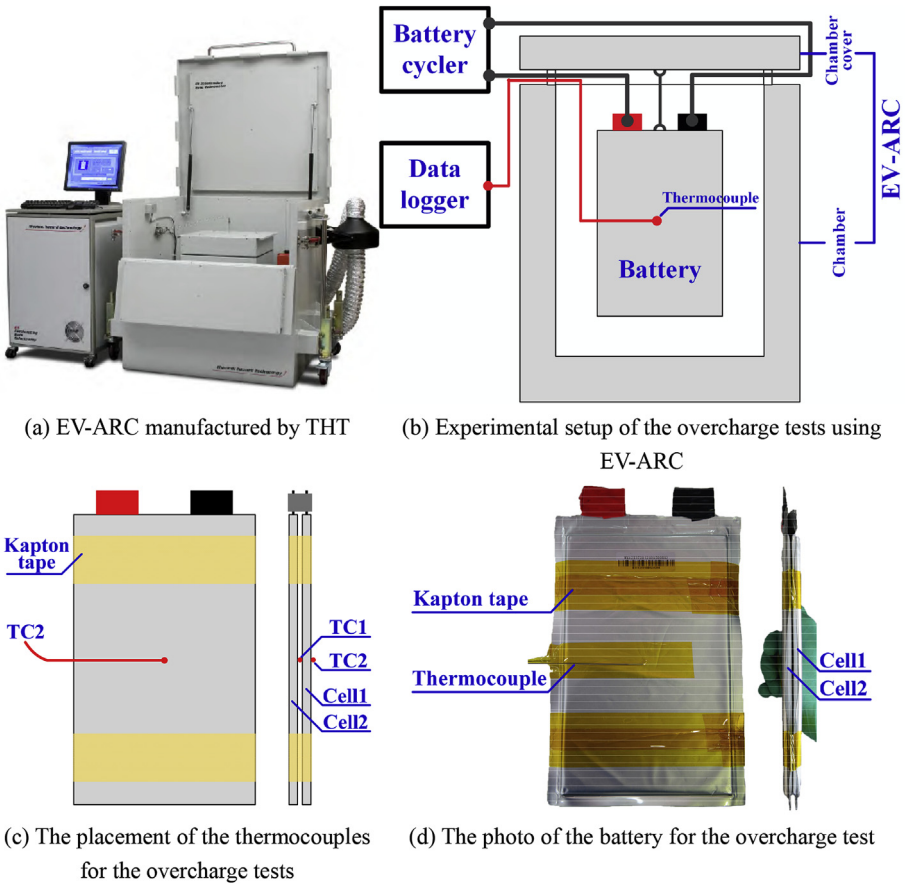

Fig. 1. The setting of the overcharge tests under adiabatic conditions using the EV-ARC.

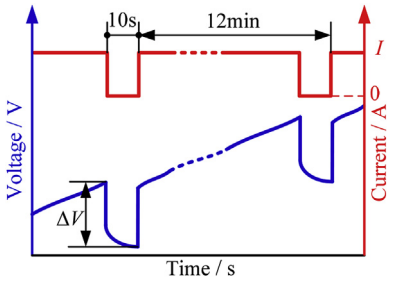

Fig. 2. Measurement of the internal resistance.

Stage I The battery voltage increases steadily and exceeds its nominal cut-off voltage at the beginning of the overcharge process. There is no obvious side reaction inside the battery at this stage, due to the excessive capacity of the cathode and the anode, as shown in Fig. 4(b). As a result, the battery temperature and internal resistance show little increase.

Stage II When the battery is overcharged to a SOC higher than 1.2, side reactions occur inside the battery, as shown in Fig. 4(c). At the cathode, the dissolution of Mn ion in the NCM + LMO composite cathode and the oxidation of the electrolyte begin under high cathode potential condition [26,27]. Meanwhile, the metallic lithium starts to deposit on the anode surface after the graphite anode is full of intercalated lithium [31]. The deposited lithium will react with solvent to thicken the SEI film, resulting in the

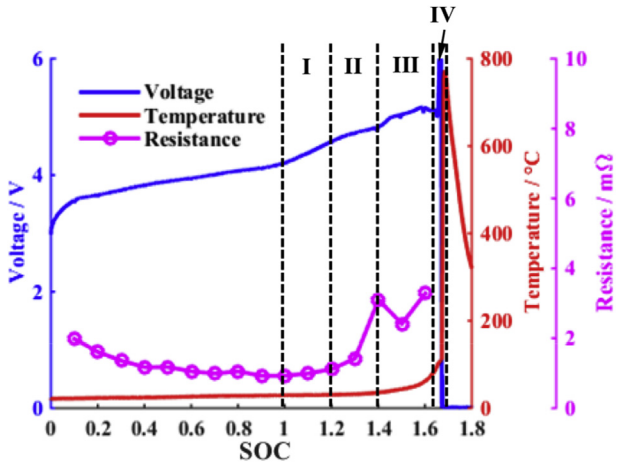

Fig. 3. The battery voltage, temperature and resistance during overcharge process.

increase of battery resistance [27,31,34]. At Stage II, the battery temperature begins to rise at a slow rate, due to heat generation from the joule heat ($Q_{ohm} = I^2 \cdot r_{bat}$) and side reactions.

Stage III The battery temperature rises more rapidly at stage III, and the battery starts to swell obviously. The oxidation of electrolyte accelerates as the cathode potential rises higher, generating a large amount of heat and gas [22,35]. Lithium deposition continues on the anode surface. At

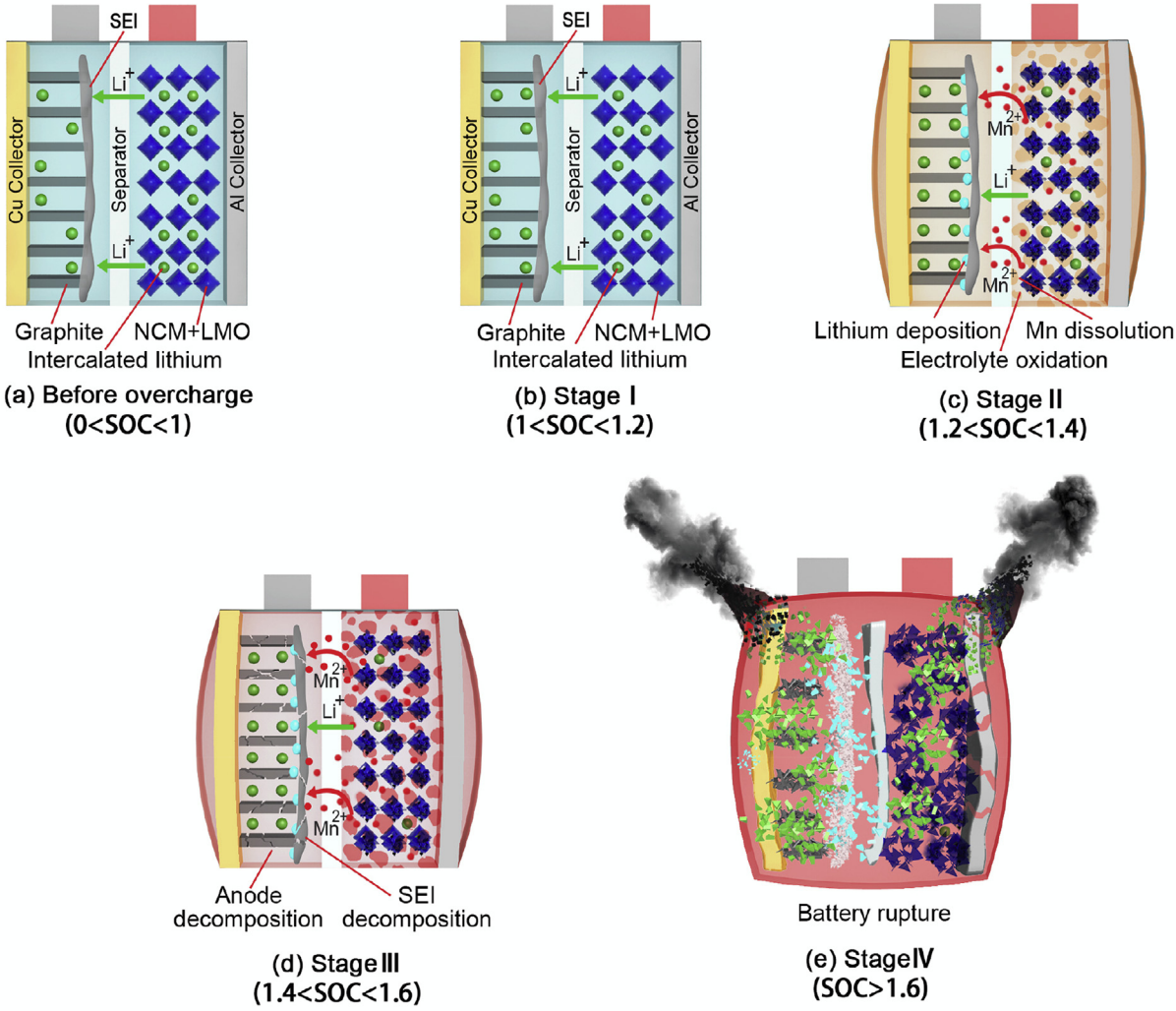

Fig. 4. Overview of the overcharge side reactions at each stages for lithium ion batteries with NCM + LMO cathode.

elevated temperature, SEI film decomposition happens, followed by the reaction between the lithiated graphite and the electrolyte [9,58], as shown in Fig. 4(d). The battery voltage shows a slight drop after peaks at around 5.2 V, mainly due to the structural change of the cathode active material [23–25,27].

Stage IV As Fig. 4(e) shows, the battery ruptures as the inner pressure exceeds its limit, resulting in the deformation of separator and thermal runaway. Fierce internal short circuit occurs, and all the energy stored inside the battery releases instantly, bringing the battery temperature peaks at around 780 °C.

3.2. Overcharge-to-thermal-runaway model

3.2.1. Electrochemical model

In this study, the battery voltage V_{sim} is modeled as the difference of the cathode potential $V_{cathode}(y)$ and anode potential $V_{anode}(x)$, with a potential increase of $I \cdot r_{bat}$, as shown in Eqn. (2) [59,60]. I is the overcharge current, and r_{bat} is the measured internal resistance of the battery during the overcharge process, as shown in Fig. 3.

$$V_{sim} = V_{cathode}(y) - V_{anode}(x) + I \cdot r_{bat} \quad (2)$$

The cathode potential $V_{cathode}(y)$ is determined by the lithium content y in the cathode active material, while the anode potential $V_{anode}(x)$ changes with the lithium content x in Li_xC_6. Fig. 5(a) and (b) show the cathode potential $V_{cathode}(y)$ varying with y and the anode potential $V_{anode}(x)$ varying with x measured in Sec. 2.2. Note that $x > 1$ in Fig. 5(b) represents that the graphite anode is over-lithiated, and the anode potential $V_{anode}(x)$ drops down to less than 0 V.

During the charging process, the lithium content y in the cathode material can be calculated by Eqn. (3), where y_0 is the initial lithium content in the cathode at the beginning of the overcharge process, and $C_{cathode}$ represents the capacity of cathode. When the battery is overcharged, $C_{cathode}$ will decrease due to dissolution and decomposition of the cathode active material, as shown in Eqn. (4). $C_{cathode,0}$ is the initial value of $C_{cathode}$, $c_{cathode}$ is the normalized concentration of cathode active material, and k_Q is the proportion factor. Likewise, the value of x can be calculated by Eqn. (5), where x_0 is the initial value of x at the beginning of the overcharge process, and C_{anode} represents the capacity of anode. It should be noted that the change of C_{anode} during the overcharge process is neglected in this model. Because when the decomposition of anode active

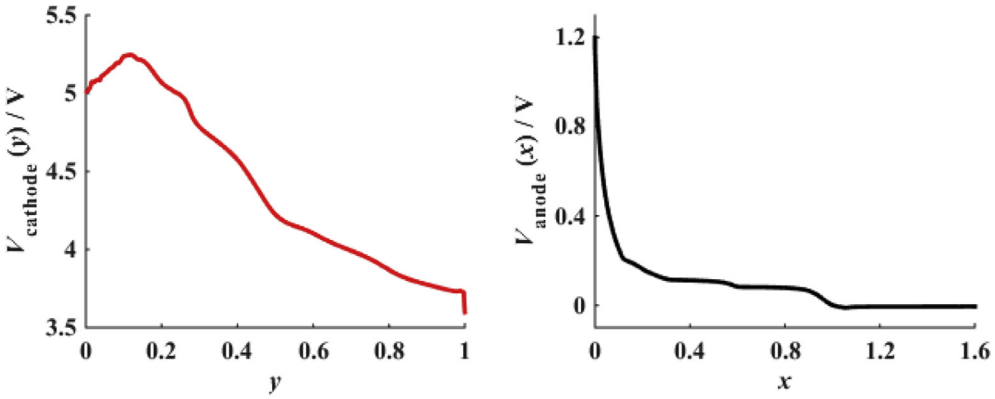

(a)The cathode potential $V_{cathode}(y)$ varying with the lithium content y in the cathode

(b)The anode potential $V_{anode}(x)$ varying with the lithium content x in Li_xC_6

Fig. 5. The cathode and anode potential with the lithium content (x, y) in the electrodes.

material occurs, the anode is severely overlithiated and the value of x is larger than 1. The anode potential $V_{anode}(x)$ remains almost constant at −0.0058 V when $x > 1$, as shown in Fig. 5(b), indicating that the decomposition of anode has little effect on the anode potential $V_{anode}(x)$. The values of the parameters used in the electrochemical model are listed in Table 2.

$$y = y_0 - I \cdot t / C_{cathode} \tag{3}$$

$$C_{cathode} = C_{cathode,0} \cdot (1\text{-}k_Q \cdot (1\text{-}c_{cathode})) \tag{4}$$

$$x = x_0 + I \cdot t / C_{anode} \tag{5}$$

3.2.2. Thermal model

A lumped thermal model is established to simulate the thermal behaviors of the battery throughout the full overcharge-to-TR process. The battery temperature can be integrated as in Eqn. (6), where T_0 is the initial temperature. The derivative of T satisfies Eqn. (7) according to the energy balance equation, where $M = 1$ kg is the mass of the battery, $C_p = 1100\ \mathrm{J\,kg^{-1}\,K^{-1}}$ is the specific heat capacity of the battery, which is measured before overcharge test using EV-ARC.

$$T(t) = T_0 + \int \frac{dT}{dt} dt \tag{6}$$

$$\frac{dT}{dt} = \frac{Q}{MC_p} \tag{7}$$

$$Q = Q_{rev} + Q_{ohm} + Q_r + Q_e - Q_p \tag{8}$$

Table 2
The parameters used in the electrochemical model.

Symbol	Description	Value
y_0	The initial lithium content in the cathode	1
$C_{cathode,0}$	The initial value of the capacity of cathode	78.5 Ah
k_Q	The proportion factor for cathode capacity	0.1
x_0	The initial lithium content in the anode	0.02
C_{anode}	The capacity of anode	52.5 Ah

Q is the total heat generation rate as in Eqn. (8), where Q_{rev} is the reversible entropic heat generation rate; Q_{ohm} is the joule heat generation rate; Q_r denotes the heat generation rate by chemical reactions; Q_e represents the heat generation released by massive internal short circuit during thermal runaway and Q_p is the heat dissipation rate. For the overcharge tests under adiabatic condition, we can set $Q_p = 0$ in our overcharge-to-TR model.

$$Q_{rev} = -I \cdot T \cdot \frac{\partial U_{OCV}}{\partial T} \tag{9}$$

The reversible heat generation rate Q_{rev} is determined by the battery overcharge current I and the effective entropic potential $T \cdot \frac{\partial U_{OCV}}{\partial T}$, as shown in Eqn. (9), where T is the battery temperature in Kelvin, and $\frac{\partial U_{OCV}}{\partial T}$ is the entropic heat coefficient. The entropic heat coefficient $\frac{\partial U_{OCV}}{\partial T}$ can be obtained by measuring the battery open circuit voltage (OCV) variation under different temperatures [61], and the results is presented in Table 3. Details of the measurement of the entropic heat coefficient $\frac{\partial U_{OCV}}{\partial T}$ of the battery can be found in Ref. [61]. It should be noted that Q_{rev} accounts for only a small percentage of the total heat generation rate and can be neglected when overcharge happens (the battery SOC exceeds 1.0) [4], so the entropic heat coefficient $\frac{\partial U_{OCV}}{\partial T}$ of the battery under a SOC higher than 1 is set as 0.

Q_{ohm} can be calculated by Eqn. (10), where I is the overcharge current, r_{bat} is the internal resistance of the battery measured during the overcharge tests.

$$Q_{ohm} = I^2 \cdot r_{bat} \tag{10}$$

Q_r is the sum of the heat generation rate of all the chemical reactions. According to the overcharge failure mechanism summarized in Sec.3.1, Q_r can be calculated by Eqn. (11), where Q_{Mn} denotes the heat generation rate by Mn dissolution; Q_{Li} denotes the heat generation rate by the reaction between deposited lithium and electrolyte; $Q_{electrolyte}$ denotes the heat generation rate by electrolyte oxidation; Q_{SEI} denotes the heat generation rate by SEI film

Table 3
The entropic heat coefficient $\frac{\partial U_{OCV}}{\partial T}$ of the battery under different SOC.

SOC	0	0.2	0.4	0.6	0.8	1.0	>1.0
$\frac{\partial U_{OCV}}{\partial T}$ /mV·K^{-1}	−0.310	−0.130	0.005	0.020	0.032	−0.059	0

decomposition; Q_{anode} denotes the heat generation rate by anode decomposition; $Q_{cathode}$ denotes the heat generation rate by cathode decomposition. $Q_{cathode}$ has two terms, $Q_{cathode,1}$ and $Q_{cathode,2}$ [43,62], as shown in Eqn. (12).

$$Q_r = Q_{Mn} + Q_{Li} + Q_{electrolyte} + Q_{SEI} + Q_{anode} + Q_{cathode} \quad (11)$$

$$Q_{cathode} = Q_{cathode,1} + Q_{cathode,2} \quad (12)$$

The heat generation rate Q_x by chemical reaction is in proportion to the reaction rate K_x, as shown in Eqn. (13), where the subscript x in Q_x can be Mn, Li, electrolyte, SEI, anode and cathode etc. ΔH_x is the enthalpy of the chemical reaction x, and m_x is the total mass of the reactants inside the battery. The reaction rate K_x usually conforms with Arrhenius Equation [4,39,42], as shown in Eqn. (14), where A_x is the frequency factor; $E_{a,x}$ is the activation energy; $R = 8.314$ J mol^{-1} K^{-1} is the ideal gas constant; $f_x(c_x)$ describes the relation between the reaction rate and the concentration of reactant c_x; g_x is the correction term of the reaction. The values of the parameters ΔH_x, m_x, A_x and $E_{a,x}$ for each reactions are listed in Table 4. It should be noted that Q_{Li} depends on both the amount of deposited lithium and the amount of electrolyte. In this paper, the enthalpy of the chemical reaction between deposited lithium and electrolyte ΔH_{Li} is set as 585.5 J g^{-1} of the electrolyte, according to the enthalpy of the reaction on a molar basis in Ref. [4], as shown in Table 4. The calculation of reaction rates for each exothermic reactions during the overcharge process is further discussed in the following paragraphs.

$$Q_x = \Delta H_x \cdot m_x \cdot K_x \quad (13)$$

$$K_x = A_x \cdot \exp\left(-\frac{E_{a,x}}{RT(t)}\right) \cdot f_x(c_x) \cdot g_x \quad (14)$$

The dissolution of Mn takes place under high cathode potential condition, following the disproportionation reaction as Eqn. (15) [63]. The dissolved Mn ion will migrate to the anode through the separator and deposit on the anode surface, which induces SEI film growth, impedance rise and generate heat [26].

$$2Mn^{3+} \rightarrow Mn^{4+} + Mn^{2+} \quad (15)$$

The reaction rate of Mn dissolution can be expressed as Eqn. (16), according to [63]. c_{Mn} is the normalized concentration of Mn^{3+} in the cathode. The amount of Mn^{3+} in the cathode would be consumed by both the dissolution reaction and the overcharge current [4], as shown in Eqn. (17), where $c_{Mn,0}$ is the initial value of c_{Mn}, $F = 96485$ C mol^{-1} is the Faraday constant, k_d is the proportion factor. The correction term $\exp\left(\alpha_{Mn} \cdot F \cdot \frac{V_{cathode} - V_{Mn,ref}}{RT}\right)$ in Eqn. (16) describes the relation between the reaction rate and the cathode potential [30], where α_{Mn} is the transfer coefficient; $V_{Mn,ref}$ is the Mn dissolution potential. The dissolution reaction will not occur until $V_{cathode}$ is higher than $V_{Mn,ref}$.

$$K_{Mn} = A_{Mn} \cdot \exp\left(-\frac{E_{a,Mn}}{RT}\right) \cdot c_{Mn}^{2/3} \cdot \exp\left(\alpha_{Mn} \cdot F \cdot \frac{V_{cathode} - V_{Mn,ref}}{RT}\right) \quad (16)$$

$$c_{Mn} = c_{Mn,0} - \int \left(K_{Mn} + k_{Mn} \cdot \frac{I}{F}\right) dt \quad (17)$$

Lithium deposition is expected to occur on the anode surface when the anode potential is lower than 0 V [31,34]. The deposited lithium will react with the electrolyte, resulting in heat generation [27,31,34]. The rate of the reaction between the deposited lithium and the electrolyte can be calculated by Eqn. (18) [4]. n_{Li} is the amount of the deposited lithium on the anode, while $c_{electrolyte}$ is the normalized concentration of the electrolyte. The parameter k_{Li} is set to a large value, to effectively make the term $\frac{k_{Li} \cdot n_{Li}}{1 + k_{Li} \cdot n_{Li}}$ equal to 1 when $n_{Li} \gg 1$, and 0 when $n_{Li} = 0$, as in Ref. [4]. The amount of deposited lithium on the anode can be calculated by Eqn. (19) [34], where v_{Li} is the proportion factor; i_{Li} is the rate of lithium deposition reaction and can be determined by a Bulter-Volmer equation, as shown in Eqn. (20). i_0 is the exchange-current for the reaction; α_c and α_a are the transfer coefficients; r_{SEI} is the resistance caused by the SEI film.

$$K_{Li} = A_{Li} \cdot \exp\left(-\frac{E_{a,Li}}{RT}\right) \cdot \frac{k_{Li} \cdot n_{Li}}{1 + k_{Li} \cdot n_{Li}} \cdot c_{electrolyte} \quad (18)$$

$$n_{Li} = \int \left(\frac{i_{Li}}{F} - v_{Li} \cdot K_{Li}\right) dt \quad (19)$$

$$i_{Li} = i_0 \cdot \left[\exp\left(-\alpha_c \cdot F \cdot \frac{V_{anode} - I \cdot r_{SEI}}{RT}\right) - \exp\left(\alpha_a \cdot F \cdot \frac{V_{anode} - I \cdot r_{SEI}}{RT}\right)\right] \quad (20)$$

$Q_{electrolyte}$ comes from electrolyte oxidation reaction on the cathode under high cathode potential condition. The rate of the electrolyte oxidation reaction is given by Eqn. (21), where $c_{electrolyte}$ is the normalized concentration of electrolyte. The electrolyte will also be consumed by the reaction between electrolyte and deposited lithium during the overcharge process, as shown in Eqn. (22). $c_{electrolyte,0}$ is the initial value of $c_{electrolyte}$ and $k_{electrolyte}$ is the proportion factor. The reaction is also influenced by the cathode potential [30], as shown in the correction term $\exp\left(\alpha_{electrolyte} \cdot F \cdot \frac{V_{cathode} + I \cdot r_{cathode} - V_{electrolyte,ref}}{RT}\right)$, where $\alpha_{electrolyte}$ is the transfer coefficient; $V_{elctrolyte,ref}$ is the oxidation potential of the electrolyte; $r_{cathode}$ the resistance caused by the film formed on the cathode surface. The oxidation reaction will not begin until $V_{cathode} + I \cdot r_{cathode} - V_{elctrolyte,ref}$ is higher than 0 V.

Table 4
The values of the parameters ΔH_x, m_x, A_x and $E_{a,x}$ for each reactions.

x	ΔH_x/J·g^{-1}	m_x/g[a]	A_x/s^{-1}	$E_{a,x}$/J·mol^{-1}
Mn	14	361.98	5.15×10^5 [63]	6.84×10^4 [63]
Li	585.5[c] [4]	170.8	4×10^{16}[b]	1.35×10^5 [42]
Electrolyte	520 [4,64]	170.8	1.2×10^{3}[b]	6.11×10^4 [65]
SEI	257 [42]	219	1.667×10^{15} [42]	1.35×10^5 [42]
Anode	1714 [42]	219	8[b]	3.4×10^4 [4]
Cathode,1	77 [62]	361.98	1.75×10^9 [62]	1.1495×10^5 [62]
Cathode,2	84 [62]	361.98	1.077×10^{12} [62]	1.588×10^5 [62]

[a] The mass of the reactants are calculated based on the components of the 40 Ah battery.
[b] The parameters that have no citations are evaluated within practical ranges to fit the experimental data according to ref. [4,47,65,66].
[c] ΔH_{Li} is set as 585.5 J g^{-1} of the electrolyte, according to the enthalpy of the reaction on a molar basis in Ref. [4].

$$K_{\text{electrolyte}} = A_{\text{electrolyte}} \cdot \exp\left(-\frac{E_{a,\text{electrolyte}}}{RT}\right) \cdot c_{\text{electrolyte}} \cdot \exp\left(\alpha_{\text{electrolyte}} \cdot F \cdot \frac{V_{\text{cathode}} + I \cdot r_{\text{cathode}} - V_{\text{electrolyte,ref}}}{RT}\right) \tag{21}$$

$$c_{\text{electrolyte}} = c_{\text{electrolyte},0} - \int \left(K_{\text{electrolyte}} + k_{\text{electrolyte}} \cdot K_{\text{Li}}\right) \mathrm{d}t \tag{22}$$

The SEI decomposition takes place when the temperature is higher than the onset temperature $T_{\text{onset,SEI}}$, and the reaction rate can be expressed as Eqn (23). c_{SEI} can be calculated by Eqn. (24), where $c_{\text{SEI},0}$ is the initial value of c_{SEI}.

$$K_{\text{SEI}} = A_{\text{SEI}} \cdot \exp\left(-\frac{E_{a,\text{SEI}}}{RT}\right) \cdot c_{\text{SEI}} \tag{23}$$

$$c_{\text{SEI}} = c_{\text{SEI},0} - \int K_{\text{SEI}} \mathrm{d}t \tag{24}$$

Once the SEI film is consumed and does not protect the anode from contacting with the electrolyte, the anode will decomposes, through reacting with the electrolyte and the binder at elevated temperature. The onset temperature of anode decomposition $T_{\text{onset,anode}}$ is set as 65 °C and the reaction rate is expressed as Eqn. (25) [42,43]. c_{anode} is the normalized concentration of anode active material and can be calculated by Eqn. (26), and $\exp\left(-\frac{c_{\text{SEI}}}{c_{\text{SEI,ref}}}\right)$ is the correction term, and $c_{\text{SEI,ref}} = 1$.

$$K_{\text{anode}} = A_{\text{anode}} \cdot \exp\left(-\frac{E_{a,\text{anode}}}{RT}\right) \cdot c_{\text{anode}} \cdot \exp\left(-\frac{c_{\text{SEI}}}{c_{\text{SEI,ref}}}\right) \tag{25}$$

$$c_{\text{anode}} = c_{\text{anode},0} - \int K_{\text{anode}} \mathrm{d}t \tag{26}$$

For the cathode, Q_{cathode} has two terms, $Q_{\text{cathode,1}}$ and $Q_{\text{cathode,2}}$ [43,62], as shown in Eqn. (27) and (28). The reaction rate $K_{\text{cathode,1}}$ and $K_{\text{cathode,2}}$ can be calculated by Eqn. (29) and Eqn. (30), respectively. The onset temperatures of the two cathode decomposition reactions are denoted as $T_{\text{onset, cathode,1}}$ and $T_{\text{onset, cathode,2}}$, respectively. And the amount of cathode material is calculated by Eqn. (31), where k_{cathode} is the proportion factor.

$$Q_{\text{cathode,1}} = \Delta H_{\text{cathode,1}} \cdot m_{\text{cathode}} \cdot K_{\text{cathode,1}} \tag{27}$$

$$Q_{\text{cathode,2}} = \Delta H_{\text{cathode,2}} \cdot m_{\text{cathode}} \cdot K_{\text{cathode,2}} \tag{28}$$

$$K_{\text{cathode,1}} = A_{\text{cathode,1}} \cdot \exp\left(-\frac{E_{a,\text{cathode,1}}}{RT}\right) \cdot c_{\text{cathode}} \cdot (1 - c_{\text{cathode}}) \tag{29}$$

$$K_{\text{cathode,2}} = A_{\text{cathode,2}} \cdot \exp\left(-\frac{E_{a,\text{cathode,2}}}{RT}\right) \cdot c_{\text{cathode}} \cdot (1 - c_{\text{cathode}}) \tag{30}$$

$$c_{\text{cathode}} = c_{\text{cathode},0} - \int \left(k_{\text{cathode}} \cdot K_{\text{Mn}} + K_{\text{cathode,1}} + K_{\text{cathode,2}}\right) \mathrm{d}t \tag{31}$$

Q_e in Eqn. (8) represents the heat generation rate from massive internal short circuit, which happens when the battery temperature is higher than the onset temperature of thermal runaway $T_{\text{onset,TR}}$. Q_e can be calculated by Eqn. (32) [43], where ΔH_e is the total electrical energy released during massive internal short circuit; Δt is the average short circuit time when thermal runaway happens. The values of $T_{\text{onset,TR}}$, ΔH_e and Δt can be determined by the results of the overcharge tests conducted in Sec. 2.1.

$$Q_e = \frac{1}{\Delta t}\left(\Delta H_e - \int Q_e \mathrm{d}t\right) \tag{32}$$

Table 5 summarizes the parameter values specified in the simulations.

4. Results and discussions

4.1. Model validation at variant overcharge currents

Model validation is carried out by comparing the model simulation results with overcharge tests at variant overcharge currents conducted in Sec.2.1. The model parameters used in the simulation are listed in Tables 2–4. Fig. 6 shows the model validation results for the overcharge-to-TR model at 0.33C, 0.5C and 1C. According to Fig. 6(a), (c) and (e), the batteries overcharged at different overcharge currents showed similar behaviors, and the onset time of thermal runaway declines with the increase of the overcharge currents. All the simulated temperature and voltage – time profiles fit well with the experimental results, as shown in Fig. 6(a), (c) and (e). The simulated and experimental temperature rate – temperature profiles for the overcharge tests at different overcharge currents are also illustrated in Fig. 6(b), (d) and (f), and the simulation results agree well with the experimental results.

SOC_{TR} which denotes the battery SOC when thermal runaway occurs, is usually used to evaluate the overcharge performance of lithium ion battery in test standards [1,67]. A higher SOC_{TR} indicates that the battery can endure a larger amount of overcharge capacity before thermal runaway. Table 6 compares the simulated SOC_{TR} and the experiment results for the overcharge tests at different charging rates. The simulation results are consistent with the experimental data, indicating that the overcharge-to-TR model can achieve a good capture of the overcharge-to-TR mechanism and predict the battery overcharge-induced TR behaviors well.

4.2. Modeling analysis of the overcharge-to-TR model

4.2.1. Investigation of heat generation rates for batteries overcharged at variant overcharge currents

The heat generation rates of each heat sources during the overcharge-to-TR process at variant overcharge currents are compared quantitatively in this section. Fig. 7(a) illustrates the total heat generation rates varying with SOC for the batteries overcharged at 0.33C, 0.5C and 1C, and the heat generation rates of each heat sources for the batteries overcharged at 0.33C, 0.5C and 1C are shown in Fig. 7(b), (c) and (d), respectively. It should be noted that $Q_{\text{cathode,1}}$ and $Q_{\text{cathode,2}}$ are not depicted in Fig. 7(b)–(d), as they will not be triggered until thermal runaway starts, and account for small portions (less than 2%) of the total heat generation compared to Q_e.

As shown in Fig. 7(a), the total heat generation rate Q increases with the rise of the overcharge currents, mainly due to the increase

Table 5
The parameters used in the overcharge-to-TR model.

Symbol	Description	Value
$c_{Mn,0}$	The initial value of the normalized concentration of Mn^{3+}	1
$c_{Li,0}$	The initial value of the amount of deposited lithium	0
$c_{electrolyte,0}$	The initial value of the normalized concentration of electrolyte	1
$c_{SEI,0}$	The initial value of the normalized concentration of SEI film	0.15
$c_{anode,0}$	The initial value of the normalized concentration of anode	0.85
$c_{cathode,0}$	The initial value of the normalized concentration of cathode	1
$c_{SEI,ref}$	The correction term for the anode decomposition reaction	1
i_0	The exchange-current for the lithium deposition reaction	10 A
k_{Mn}	The proportion factor for the Mn dissolution reaction	0.17
k_{Li}	The proportion factor for the lithium deposition reaction	2000
$k_{electrolyte}$	The proportion factor for the electrolyte oxidation reaction	1.75
$k_{cathode}$	The proportion factor for the cathode decomposition reaction	0.25
r_{SEI}	The resistance caused by the SEI film	0.001Ω
$r_{cathode}$	The resistance caused by the film formed on the cathode surface	0.0036Ω
$V_{Mn,ref}$	The dissolution potential of Mn^{3+}	4.35 V
$V_{electrolyte,ref}$	The oxidation potential of the electrolyte	4.46 V
$T_{onset,SEI}$	The onset temperature of SEI film decomposition reaction	40 °C
$T_{onset,anode}$	The onset temperature of the anode decomposition reaction	65 °C
$T_{onset,cathode,1}$	The onset temperature of the first cathode decomposition reaction	180 °C
$T_{onset,cathode,2}$	The onset temperature of the second cathode decomposition reaction	220 °C
ΔH_e	The total electrical energy released during massive ISC	5.0×10^5J
Δt	The average short circuit time	24s
$T_{onset,TR}$	The onset temperature of thermal runaway	110 °C
α_{Mn}	The transfer coefficient for the Mn dissolution reaction	0.41
α_c	The transfer coefficient for the lithium deposition reaction	0.7
α_a	The transfer coefficient for the lithium deposition reaction	0.3
$\alpha_{electrolyte}$	The transfer coefficient for the electrolyte oxidation reaction	0.31
v_{Li}	the proportion factor for the calculation of the amount of deposited lithium	1 mol

of the joule heat generation rate Q_{ohm}. The total heat generation rate Q roughly equals the joule heat generation rate Q_{ohm} until SOC goes higher than 1.2, as shown Fig. 7(b)–(d). The heat generation rates by chemical reactions (Q_{Mn}, Q_{Li} and $Q_{electrolyte}$) start to increase after SOC is higher than 1.2 for the overcharge tests at 0.33C and 0.5C, as shown in Fig. 7(b) and (c), while chemical reactions happen at a lower SOC (around 1.14) for the overcharge test at 1C, as shown in Fig. 7(d). $Q_{electrolyte}$ exceeds Q_{ohm} and becomes the dominant heat source when SOC reaches around 1.45 for all of the overcharge tests at 0.33C, 0.5C and 1C. As the overcharge process continues, Q_{Li} increases sharply and results in the total heat generation rate peaking at around 100 W when SOC goes higher than 1.60. Meanwhile, Q_{SEI} and Q_{anode} are also released at elevated temperature. In general, $Q_{electrolyte}$ and Q_{Li} are the two dominant heat sources during the overcharge process until the temperature reaches $T_{onset,TR} = 110$ °C and thermal runaway happens. Therefore, to improve the overcharge safety of lithium ion battery, efforts should be paid to reducing $Q_{electrolyte}$ and Q_{Li}.

4.2.2. Modeling analysis of critical parameters

Modeling analysis has been performed on the critical parameters to investigate their influence on the battery overcharge performance in this section, which can help to find solutions to improve the battery overcharge safety.

According to the results in Sec.4.2.1, $Q_{electrolyte}$ and Q_{Li} are the two dominant heat sources during the overcharge process. $Q_{electrolyte}$ is generated by the electrolyte oxidation, and the reaction rate is determined by Eqn. (21). Q_{Li} comes from the reaction between deposited lithium and electrolyte, and the reaction rate mainly depends on the amount of deposited lithium according to Eqn (18). Moreover, the onset temperature of thermal runaway $T_{onset,TR}$ also affects the overcharge safety of lithium ion battery. Therefore, for the modeling analysis, we can adjust three critical parameters: (1) $V_{electrolyte,ref}$, which denotes the oxidation potential of the electrolyte and will influence the generation of $Q_{electrolyte}$; (2) C_{anode}, which denotes the capacity of anode and will affect the lithium deposition reaction; (3) $T_{onset,TR}$, which denotes the onset temperature of thermal runaway. And the variation of SOC_{TR} for different parameters can be obtained by calculating the ratio between the amount of accumulative charging capacity before TR happens and the normalized battery capacity.

$V_{electrolyte,ref}$ denotes the oxidation potential of the electrolyte, which reflects the stability of electrolyte at high cathode potential. Fig. 8(a) illustrates the variation of SOC_{TR} for different $V_{electrolyte,ref}$ predicted by the overcharge-to-TR model. SOC_{TR} shows an obvious rise (from 1.6 to 1.85) when increasing $V_{electrolyte,ref}$ from 4.4 V to 5 V, as the generation of $Q_{electrolyte}$ is postponed and the battery temperature rise is thus slowed down. This indicates that using electrolyte with a high $V_{electrolyte,ref}$ can significantly improve the overcharge safety of lithium ion battery. Furthermore, the change of SOC_{TR} with the rising of $V_{electrolyte,ref}$ can be divided into two sections, as shown in Fig. 8(a). In section 1, SOC_{TR} rises rapidly when increasing $V_{electrolyte,ref}$ from 4.4 V to 4.7 V, while it shows minor change (from 1.83 to 1.85) when increasing $V_{electrolyte,ref}$ from 4.7 V to 5 V in section 2. Thus, 4.7 V, which is the boundary of the two sections, can be considered as the optimal value of $V_{electrolyte,ref}$. The oxidation potential of the electrolyte can be increased by adding functional additives or developing novel high-voltage stable solvents [68]. Electrolyte oxidation can also be prevented by adding redox shuttle additive in the electrolyte to achieve a current bypass mechanism and stop the continuous rise of battery voltage during overcharge [3,27,69].

C_{anode} represents the capacity of anode, and was set as 52.5 Ah in the simulations, as shown in Table 2. The value of C_{anode} will influence the deposition of metallic lithium, which usually happens when the anode is fully lithiated. Excess anode active material is used in commercial lithium ion batteries to prevent lithium deposition at the end of charging [11,34]. The influence of C_{anode} on the value of SOC_{TR} is shown in Fig. 8(b). A larger C_{anode} indicates that more anode active material is used in the battery, resulting in later occurrence of lithium deposition [11,34]. However, SOC_{TR} shows minor change with the increase of C_{anode} and remains stable

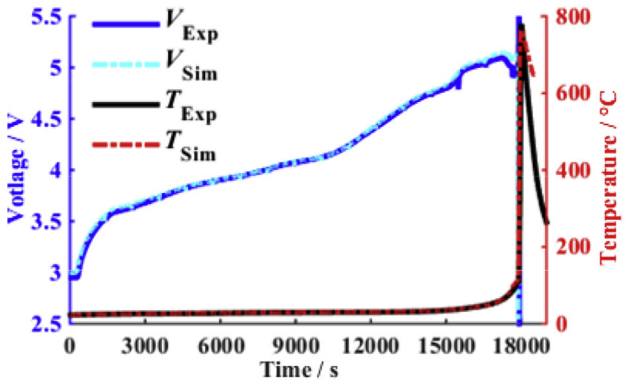

(a)Temperature and voltage vs. time for overcharge test at 0.33C

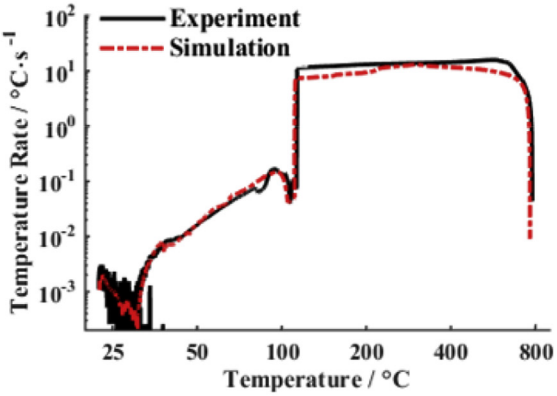

(b) Temperature rate vs. temperature for overcharge test at 0.33C

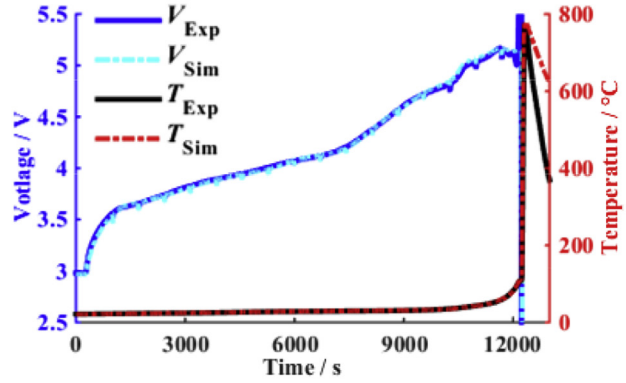

(c) Temperature and voltage vs. time for overcharge test at 0.5C

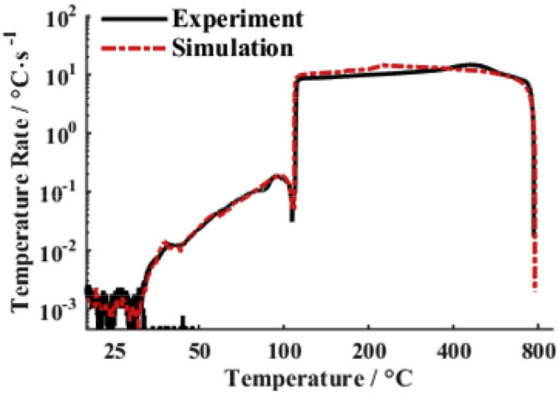

(d) Temperature rate vs. temperature for overcharge test at 0.5C

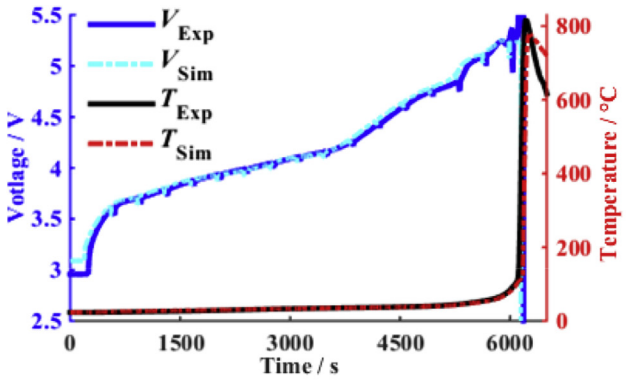

(e) Temperature and voltage vs. time for overcharge test at 1C

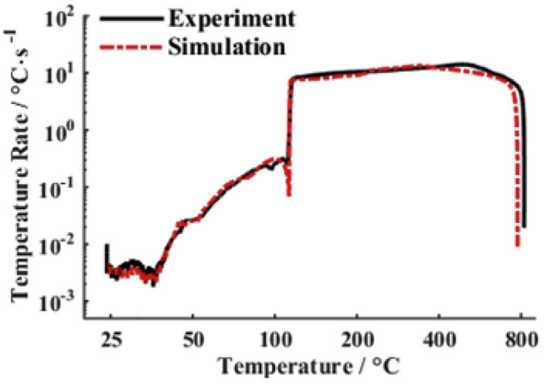

(f) Temperature rate vs. temperature for overcharge test at 1C

Fig. 6. Comparison of the model simulation and the overcharge tests at variant overcharge currents.

Table 6
Comparison of the SOC_{TR} for the model and experiment.

Charging rate		0.33C	0.5C	1C
SOC_{TR}	Experiment	1.674	1.670	1.652
	Simulation	1.678	1.671	1.656

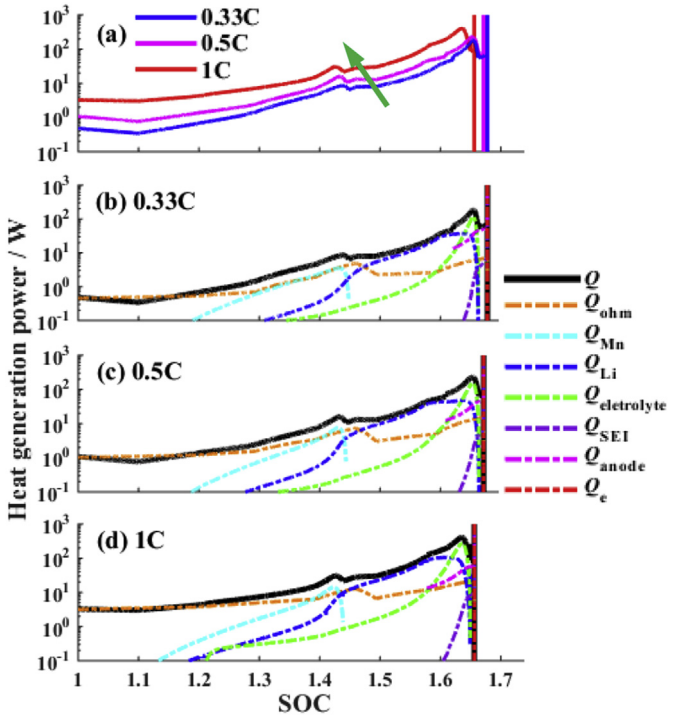

Fig. 7. (a) Comparison of heat generation rate for batteries overcharged at variant overcharge currents; (b) the heat generation rates of each heat sources for the batteries overcharged at 0.33C; (c) the heat generation rates of each heat sources for the batteries overcharged at 0.5C; (d) the heat generation rates of each heat sources for the batteries overcharged at 1C.

at around 1.71 when C_{anode} is higher than 68 Ah (130% of its original value), as shown in Fig. 8(b). This indicates that increasing the amount of anode active material has little effect on the overcharge safety of lithium ion batteries, consistent with the results in Refs. [11,16,17].

$T_{onset,TR}$ denotes the onset temperature of thermal runaway during overcharge process. SOC_{TR} rises gradually from 1.65 to around 1.80 as $T_{onset,TR}$ increases from 100 °C to 300 °C, as shown in Fig. 8(c), indicating that the battery can endure higher temperature and show better overcharge performance. For the pouch lithium ion battery investigated in this research, the onset of thermal runaway during overcharge process is mainly caused by the rapture of the battery, as discussed in Sec.3.1. Thus, $T_{onset,TR}$ can be increased by reducing the amount of gas generated during overcharge process or proper design of the pressure release valve [27]. Moreover, a thermal stable separator should be applied to improve the overcharge safety as thermal runaway will also be triggered by the collapse of the separator and sequent massive internal short circuit at elevated temperatures [70].

5. Conclusion

In this paper, an electrochemical-thermal coupled overcharge-to-TR model for lithium ion battery is firstly established to predict the electrochemical and thermal behaviors of lithium ion battery during overcharge-to-TR process. Overcharge tests at variant overcharge currents (0.33C, 0.5C and 1C) were conducted under adiabatic conditions using EV-ARC to verify the model. The model can fit well with the experimental data, as all the simulated temperature and voltage – time profiles agree well with the experimental results at variant overcharge currents. And all the simulated SOC_{TR} is also consistent with the experiment results, indicating a good capture of the overcharge-to-thermal-runaway mechanism.

With the help of the overcharge-to-TR model, the heat generation rates of each heat sources during the overcharge-to-TR process at variant overcharge currents are compared quantitatively. The results show that $Q_{electrolyte}$ and Q_{Li} are the two dominant heat sources during the overcharge process before thermal runaway happens. Therefore, we can improve the overcharge safety of lithium ion battery through reducing $Q_{electrolyte}$ and Q_{Li}.

Modeling analysis is performed on three critical parameters ($V_{electrolyte,ref}$, C_{anode} and $T_{onset,TR}$) to investigate their influences on the battery overcharge performance and find possible solutions for the battery overcharge safety problem. Increasing the oxidation potential of the electrolyte and increasing the onset temperature of thermal runaway are found to be the two effective ways to improve the overcharge performance of lithium ion battery, as SOC_{TR} shows an obvious rise when $V_{electrolyte,ref}$ and $T_{onset,TR}$ are increased. And the optimal $V_{electrolyte,ref}$ can be found on the boundary of the two sections of the $V_{electrolyte,ref}$ – SOC_{TR} profile, as SOC_{TR} stays almost constant in section 2. However, SOC_{TR} shows minor change with the increase of C_{anode}, indicating that increasing the amount of anode active material shows little effect on the overcharge safety of lithium ion batteries.

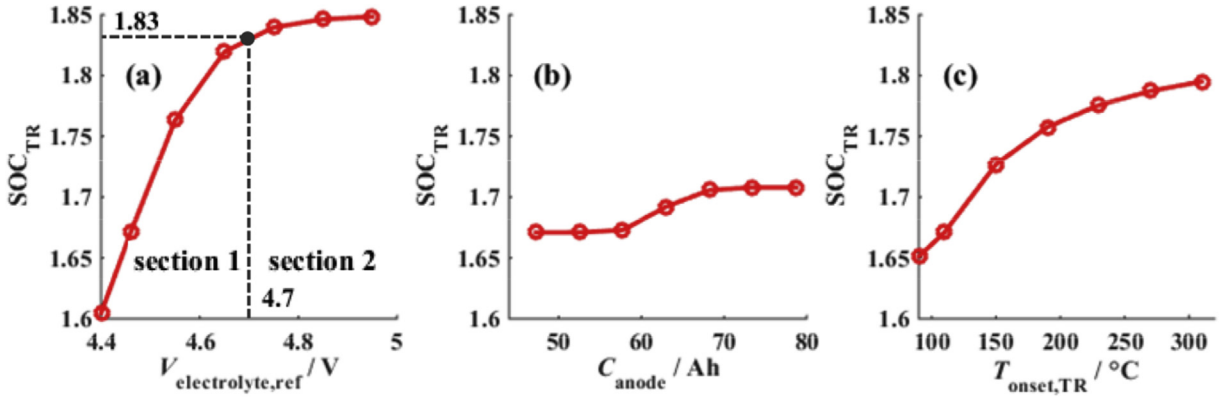

Fig. 8. The influence of three critical parameters on battery overcharge performance. (a) the variation of SOC_{TR} for different $V_{electrolyte,ref}$; (a) the variation of SOC_{TR} for different C_{anode}; (a) the variation of SOC_{TR} for different $T_{onset,TR}$.

Acknowledgement

This work is supported by the National Natural Science Foundation of China under the Grant No. U1564205, and funded by the International Science & Technology Cooperation Program of China under the Grant No. 2016YFE0102200.

References

[1] D.H. Doughty, A.A. Pesaran, Vehicle Battery Safety Roadmap Guidance, 2012.
[2] Q. Wang, P. Ping, X. Zhao, G. Chu, J. Sun, C. Chen, Thermal runaway caused fire and explosion of lithium ion battery, J. Power Sourc. 208 (2012) 210–224.
[3] J. Wen, Y. Yu, C. Chen, A review on lithium-ion batteries safety issues: existing problems and possible solutions, Mater. Express 2 (2012) 197–212.
[4] R. Spotnitz, J. Franklin, Abuse behavior of high-power, lithium-ion cells, J. Power Sourc. 113 (2003) 81–100.
[5] S. Abada, G. Marlair, A. Lecocq, M. Petit, V. Sauvant-Moynot, F. Huet, Safety focused modeling of lithium-ion batteries: a review, J. Power Sourc. 306 (2016) 178–192.
[6] X. Feng, M. Ouyang, X. Liu, L. Lu, Y. Xia, X. He, Thermal runaway mechanism of lithium ion battery for electric vehicles: a review, Energy Storage Mater, http://dx.doi.org/10.1016/j.ensm.2017.05.013.
[7] Y. Xia, T. Wierzbicki, E. Sahraei, X. Zhang, Damage of cells and battery packs due to ground impact, J. Power Sourc. 267 (2014) 78–97.
[8] F. Larsson, B.-E. Mellander, Abuse by external heating, overcharge and short circuiting of commercial lithium-ion battery cells, J. Electrochem. Soc. 161 (2014) A1611–A1617.
[9] E.P. Roth, D.H. Doughty, Thermal abuse performance of high-power 18650 Li-ion cells, J. Power Sourc. 128 (2004) 308–318.
[10] Q. Wang, X. Zhao, J. Ye, Q. Sun, P. Ping, J. Sun, Thermal response of lithium-ion battery during charging and discharging under adiabatic conditions, J. Therm. Anal. Calorim 124 (2016) 417–428.
[11] Y. Zeng, K. Wu, D. Wang, Z. Wang, L. Chen, Overcharge investigation of lithium-ion polymer batteries, J. Power Sourc. 160 (2006) 1302–1307.
[12] J. Ye, H. Chen, Q. Wang, P. Huang, J. Sun, S. Lo, Thermal behavior and failure mechanism of lithium ion cells during overcharge under adiabatic conditions, Appl. Energy 182 (2016) 464–474.
[13] M. Ouyang, D. Ren, L. Lu, J. Li, X. Feng, X. Han, et al., Overcharge-induced capacity fading analysis for large format lithium-ion batteries with $Li_yNi_{1/3}Co_{1/3}Mn_{1/3}O_2$+$Li_yMn_2O_4$ composite cathode, J. Power Sourc. 279 (2015) 626–635.
[14] L. Lu, X. Han, J. Li, J. Hua, M. Ouyang, A review on the key issues for lithium-ion battery management in electric vehicles, J. Power Sourc. 226 (2013) 272–288.
[15] Q. Yuan, F. Zhao, W. Wang, Y. Zhao, Z. Liang, D. Yan, Overcharge failure investigation of lithium-ion batteries, Electrochim. Acta 178 (2015) 682–688.
[16] R.A. Leising, M.J. Palazzo, E.S. Takeuchi, K.J. Takeuchi, A study of the overcharge reaction of lithium-ion batteries, J. Power Sourc. 97–98 (2001) 681–683.
[17] R.A. Leising, M.J. Palazzo, E.S. Takeuchi, K.J. Takeuchi, Abuse testing of lithium-ion batteries: characterization of the overcharge reaction of $LiCoO_2$/graphite cells, J. Electrochem. Soc. 148 (2001) A838–A844.
[18] F. Xu, H. He, Y. Liu, C. Dun, Y. Ren, Q. Liu, et al., Failure investigation of $LiFePO_4$ cells under overcharge conditions, ECS Trans. 41 (2012) 1–12.
[19] D. Belov, M.H. Yang, Failure mechanism of Li-ion battery at overcharge conditions, J. Solid State Electrochem 12 (2008) 885–894.
[20] D. Belov, M.H. Yang, Investigation of the kinetic mechanism in overcharge process for Li-ion battery, Solid State Ionics 179 (2008) 1816–1821.
[21] P. Biensan, B. Simon, J. Pérès, A. de Guibert, M. Broussely, J. Bodet, et al., On safety of lithium-ion cells, J. Power Sourc. 81–82 (1999) 906–912.
[22] T. Ohsaki, T. Kishi, T. Kuboki, N. Takami, N. Shimura, Y. Sato, et al., Overcharge reaction of lithium-ion batteries, J. Power Sourc. 146 (2005) 97–100.
[23] Y.B. He, F. Ning, Q.H. Yang, Q.S. Song, B. Li, F. Su, et al., Structural and thermal stabilities of layered $Li(Ni_{1/3}Co_{1/3}Mn_{1/3})O_2$ materials in 18650 high power batteries, J. Power Sourc. 196 (2011) 10322–10327.
[24] C.K. Lin, Y. Ren, K. Amine, Y. Qin, Z. Chen, In situ high-energy X-ray diffraction to study overcharge abuse of 18650-size lithium-ion battery, J. Power Sourc. 230 (2013) 32–37.
[25] L. Wu, K.W. Nam, X. Wang, Y. Zhou, J.C. Zheng, X.Q. Yang, et al., Structural origin of overcharge-induced thermal instability of Ni-containing layered-cathodes for high-energy-density lithium batteries, Chem. Mater 23 (2011) 3953–3960.
[26] H. Zheng, Q. Sun, G. Liu, X. Song, V.S. Battaglia, Correlation between dissolution behavior and electrochemical cycling performance for $LiNi_{1/3}Co_{1/3}Mn_{1/3}O_2$-based cells, J. Power Sourc. 207 (2012) 134–140.
[27] P. Arora, R.E. White, M. Doyle, Capacity fade mechanisms and side reactions in lithium-ion batteries, J. Electrochem. Soc. 145 (1998) 3647–3667.
[28] K. Qian, Y. Li, Y. He, D. Liu, Y. Zheng, L. Dan, et al., Abuse tolerance behavior of layered oxide-based Li-ion battery during overcharge and over-discharge, RSC Adv. 6 (2016) 76897–76904.
[29] Y. Liu, J. Xie, Failure study of commercial LiFePO 4 cells in overcharge conditions using electrochemical impedance spectroscopy, J. Electrochem. Soc. 162 (2015) A2208–A2217.
[30] R. Darling, J. Newman, Modeling side reactions in composite $LiMn_2O_4$ electrodes, J. Electrochem. Soc. 145 (1998) 990–998.
[31] N. Sharma, V.K. Peterson, Overcharging a lithium-ion battery: effect on the Li_xC_6 negative electrode determined by in situ neutron diffraction, J. Power Sourc. 244 (2012) 1–7.
[32] Q. Liu, C. Du, B. Shen, P. Zuo, X. Cheng, Y. Ma, et al., Understanding of undesirable anode lithium plating issues in lithium-ion batteries, RSC Adv. 6 (2016) 88683–88700.
[33] J. Arai, Y. Okada, K. Gotoh, In situ solid state ^{7}Li NMR observation of lithium metal deposition during overcharge of lithium ion battery, J. Electrochem. Soc. 162 (2015) A952–A958.
[34] P. Arora, M. Doyle, R.E. White, Mathematical modeling of the lithium deposition overcharge reaction in lithium-ion batteries using carbon-based negative electrodes, J. Electrochem. Soc. 146 (1999) 3543–3553.
[35] K. Kumai, H. Miyashiro, Y. Kobayashi, K. Takei, R. Ishikawa, Gas generation mechanism due to electrolyte decomposition in commercial lithium-ion cell, J. Power Sourc. 81–82 (1999) 715–719.
[36] S. Tobishima, J. Yamaki, A consideration of lithium cell safety, J. Power Sourc. 81–82 (1999) 882–886.
[37] G.-H. Kim, K. Smith, K.-J. Lee, S. Santhanagopalan, A. Pesaran, Multi-domain modeling of lithium-ion batteries encompassing multi-physics in varied length scales, J. Electrochem. Soc. 158 (2011) A955–A969.
[38] P.T. Coman, S. Rayman, R.E. White, A lumped model of venting during thermal runaway in a cylindrical Lithium Cobalt Oxide lithium-ion cell, J. Power Sourc. 307 (2016) 56–62.
[39] T.D. Hatchard, D.D. MacNeil, A. Basu, J.R. Dahn, Thermal model of cylindrical and prismatic lithium-ion cells, J. Electrochem. Soc. 148 (2001) A755–A761.
[40] A.A. Pesaran, Battery thermal models for hybrid vehicle simulations, J. Power Sourc. 110 (2002) 377–382.
[41] W. Zhao, G. Luo, C.-Y. Wang, Modeling nail penetration process in large-format Li-Ion cells, J. Electrochem. Soc. 162 (2014) A207–A217.
[42] G.-H. Kim, A. Pesaran, R. Spotnitz, A three-dimensional thermal abuse model for lithium-ion cells, J. Power Sourc. 170 (2007) 476–489.
[43] X. Feng, X. He, M. Ouyang, L. Lu, P. Wu, C. Kulp, et al., Thermal runaway propagation model for designing a safer battery pack with 25Ah $LiNi_xCo_yMn_zO_2$ large format lithium ion battery, Appl. Energy 154 (2015) 74–91.
[44] X. Feng, L. Lu, M. Ouyang, J. Li, X. He, A 3D thermal runaway propagation model for a large format lithium ion battery module, Energy 115 (2016) 194–208.
[45] Q. Wang, P. Ping, J. Sun, Catastrophe analysis of cylindrical lithium ion battery, Nonlinear Dyn. 61 (2010) 763–772.
[46] P. Huang, P. Ping, K. Li, H. Chen, Q. Wang, J. Wen, et al., Experimental and modeling analysis of thermal runaway propagation over the large format energy storage battery module with Li4Ti5O12 anode, Appl. Energy 183 (2016) 659–673.
[47] M.N. Richard, J.R. Dahn, Accelerating rate calorimetry study on the thermal stability of lithium intercalated graphite in electrolyte. II. Modeling the results and predicting differential scanning calorimeter curves, J. Electrochem. Soc. 146 (1999) 2078–2084.
[48] M.N. Richard, J.R. Dahn, Accelerating rate calorimetry study on the thermal stability of lithium intercalated graphite in electrolyte. I. Experimental, J. Electrochem. Soc. 146 (1999) 2068–2077.
[49] D.D. MacNeil, J.R. Dahn, Test of reaction kinetics using both differential scanning and accelerating rate calorimetries as applied to the reaction of $LixCoO_2$ in non-aqueous electrolyte, J. Phys. Chem. A 105 (2001) 4430–4439.
[50] Q. Wang, J. Sun, X. Yao, C. Chen, Thermal behavior of lithiated graphite with electrolyte in lithium-ion batteries, J. Electrochem. Soc. 153 (2006) A329–A333.
[51] G. Liang, Y. Zhang, Q. Han, Z. Liu, Z. Jiang, S. Tian, A novel 3D-layered electrochemical-thermal coupled model strategy for the nail-penetration process simulation, J. Power Sour.c 342 (2017) 836–845.
[52] C. Zhang, S. Santhanagopalan, M.A. Sprague, A.A. Pesaran, Coupled mechanical-electrical-thermal modeling for short-circuit prediction in a lithium-ion cell under mechanical abuse, J. Power Sourc. 290 (2015) 102–113.
[53] C. Zhang, S. Santhanagopalan, M.A. Sprague, A.A. Pesaran, A representative-sandwich model for simultaneously coupled mechanical-electrical-thermal simulation of a lithium-ion cell under quasi-static indentation tests, J. Power Sourc. 298 (2015) 309–321.
[54] J. Xu, B. Liu, X. Wang, D. Hu, Computational model of 18650 lithium-ion battery with coupled strain rate and SOC dependencies, Appl. Energy 172 (2016) 180–189.
[55] J. Xu, Y. Wu, S. Yin, Investigation of effects of design parameters on the internal short-circuit in cylindrical lithium-ion batteries, RSC Adv. 7 (2017) 14360–14371.
[56] X. Feng, C. Weng, M. Ouyang, J. Sun, Online internal short circuit detection for a large format lithium ion battery, Appl. Energy 161 (2016) 168–180.
[57] G.H. Kim, K. Smith, J. Ireland, A. Pesaran, Fail-safe design for large capacity lithium-ion battery systems, J. Power Sourc. 210 (2012) 243–253.
[58] X. Feng, M. Fang, X. He, M. Ouyang, L. Lu, H. Wang, et al., Thermal runaway features of large format prismatic lithium ion battery using extended volume accelerating rate calorimetry, J. Power Sourc. 255 (2014) 294–301.
[59] X. Han, M. Ouyang, L. Lu, J. Li, Y. Zheng, Z. Li, A comparative study of commercial lithium ion battery cycle life in electrical vehicle: aging mechanism identification, J. Power Sourc. 251 (2014) 38–54.
[60] M. Ouyang, X. Feng, X. Han, L. Lu, Z. Li, X. He, A dynamic capacity degradation

model and its applications considering varying load for a large format Li-ion battery, Appl. Energy 165 (2016) 48–59.
[61] G. Liu, M. Ouyang, L. Lu, J. Li, X. Han, Analysis of the heat generation of lithium-ion battery during charging and discharging considering different influencing factors, J. Therm. Anal. Calorim. 116 (2014) 1001–1010.
[62] H. Wang, A. Tang, K. Huang, Oxygen Evolution in overcharge $LixNi_{1/3}Co_{1/3}Mn_{1/3}O_2$ electrode and its thermal analysis kinetics, Chin. J. Chem. 29 (2011) 1583–1588.
[63] C.-H. Lu, S.-W. Lin, Dissolution kinetics of spinel lithium manganate and its relation to capacity fading in lithium ion batteries, J. Mater. Res. 17 (2002) 1476–1481.
[64] T. Kawamura, A. Kimura, M. Egashira, S. Okada, J.I. Yamaki, Thermal stability of alkyl carbonate mixed-solvent electrolytes for lithium ion cells, J. Power Sourc. 104 (2002) 260–264.
[65] C. Lampe-Onnerud, R. Chamberlain, P. Onnerud, Safety studies of Li-ion key components by ARC, Proc. Sixt. Annu. Batter. Conf. Appl. Adv. (2001) 367–373.
[66] P. Ping, Q. Wang, P. Huang, J. Sun, C. Chen, Thermal behaviour analysis of lithium-ion battery at elevated temperature using deconvolution method, Appl. Energy 129 (2014) 261–273.
[67] D.H. Doughty, SAE J2464 "EV & HEV Rechargeable Energy Storage System (RESS) Safety and Abuse Testing Procedure," SAE Int, 2010.
[68] M. Hu, X. Pang, Z. Zhou, Recent progress in high-voltage lithium ion batteries, J. Power Sourc. 237 (2013) 229–242.
[69] S.A. Odom, S. Ergun, P.P. Poudel, S.R. Parkin, A fast, inexpensive method for predicting overcharge performance in lithium-ion batteries, Energy Environ. Sci. 7 (2014) 760–767.
[70] P. Arora, Z. Zhang, Battery separators, Chem. Rev. 104 (2004) 4419–4462.